

Automating Perforator Flap MRA and CTA Reporting

Christopher J. Lange^{1,2} · Nanda Deepa Thimmappa¹ · Srikanth R. Boddu¹ ·
Silvina P. Dutruel¹ · Mengchao Pei¹ · Zerwa Farooq¹ · Ashkan Heshmatzadeh Behzadi¹ ·
Yi Wang¹ · Ramin Zabih^{1,2,3} · Martin R. Prince^{1,4}

Published online: 17 January 2017
© Society for Imaging Informatics in Medicine 2017

Abstract Surgical breast reconstruction after mastectomy requires precise perforator coordinates/dimensions, perforator course, and fat volume in a radiology report. Automatic perforator reporting software was implemented as an OsiriX Digital Imaging and Communications in Medicine (DICOM) viewer plugin. For perforator analysis, the user identifies a reference point (e.g., umbilicus) and marks each perforating artery/vein bundle with multiple region of interest (ROI) points along its course beginning at the muscle–fat interface. Computations using these points and analysis of image data produce content for the report. Post-processing times were compared against conventional/manual methods using de-identified images of 26 patients with surgically confirmed accuracy of perforator locations and caliber. The time from loading source images to completion of report was measured. Significance of differences in mean processing times for this automated approach versus the conventional/manual approach was assessed using a paired *t* test. The mean conventional reporting time for our radiologists was 76 ± 27 min (median 65 min) compared with 25 ± 6 min (median 25 min) using our OsiriX plugin ($p < 0.01$). The conventional approach had three reports with transcription errors compared to none with the OsiriX plugin. Otherwise, the reports were

similar. In conclusion, automated reporting of perforator magnetic resonance angiography (MRA) studies is faster compared with the standard, manual approach, and transcription errors which are eliminated.

Keywords Breast reconstruction · Magnetic resonance angiography · Computed tomographic angiography · Perforator · Autologous flap · Automated reporting

Background

Surgical breast reconstruction after mastectomy is a vital component of the overall breast cancer treatment plan to restore breast symmetry and quality of life. Breast reconstruction can be performed using a prosthesis or autologous tissue. One type of autologous tissue transfer utilizes the patient's own skin and fat harvested from abdomen, back, buttock, or posterior thigh together with a vascular pedicle to reconstruct a natural breast. The vascular pedicle is a perforating artery/vein bundle (Fig. 1); hence, they are called perforator flap reconstructions. These “perforator flaps” are vascularized by the deep inferior epigastric artery (DIEA), superior/inferior gluteal arteries (SGA/IGA), circumflex iliac, lumbar, or profunda femoral artery which can be anastomosed to the internal mammary or thoracodorsal artery. The tissue-harvesting procedure for free perforator flap involves careful dissection of the skin and subcutaneous fat along with an artery/vein bundle responsible for flap perfusion and venous drainage. Due to wide variations in patient perforator anatomy, intra-operative selection of a vascular pedicle artery/vein bundle to provide adequate arterial perfusion and venous drainage is time consuming and depends on visual evaluation during the surgery. Pre-operative imaging of donor sites to map perforator artery

✉ Martin R. Prince
map2008@med.cornell.edu

¹ Department of Radiology, Weill Medical College of Cornell University, New York, NY, USA

² Department of Computer Science, Cornell University, Ithaca, NY, USA

³ Google, New York, NY, USA

⁴ Department of Radiology, Columbia University, New York, NY, USA

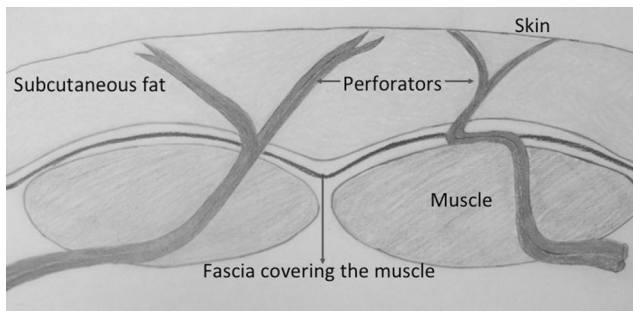


Fig. 1 Cross-sectional illustration demonstrating a perforator supplying a flap of skin and fat, referred to as “perforator flap”

anatomy improves the efficiency of perforator selection/harvesting, reducing operating room time and complications [1, 2].

Both computed tomographic angiography (CTA) with iodinated contrast agents and magnetic resonance angiography (MRA) with blood pool gadolinium contrast agents accurately map perforator arteries [3, 4]. A substantial part of pre-operative assessment is post-processing the CTA or MRA image data to provide information on the number of perforating vessels available, their diameter, location relative to well-defined surface landmarks, intramuscular course and length, and estimated flap volumes [5]. Volume-rendered three-dimensional (3D) maps of perforating vessel locations and maximum intensity projection (MIP) images of each vessel are requested by the surgeons to facilitate localization of the perforator arteries during pre-operative skin marking and intra-operatively. From reading the MRA/CTA to the generation of a report, the process takes up to 2 h at our institution to prepare using standard radiological reporting tools.

Here, we develop and test a new reporting tool on perforator flap MRA studies implemented as an OsiriX plugin, which automates perforator flap reporting, making it less time consuming and eliminating the possibility of transcription errors.

Methods

Retrospective review of existing patient data in the Picture Archiving Computer System (PACS) identified MRA perforator flap images that were anonymized for this research. Due to concern for ionizing radiation with CTA [6] and excellent vessel-to-muscle contrast with MRA [2], MRA imaging is preferred at our institution. Retrospective review of these patients’ clinical records was approved by the local institutional review board, and this study is HIPPA compliant. All MRA studies were acquired on a 1.5T magnet (GE Signa 15.0/14.0, Milwaukee, WI) using an 8-channel phased array coil/cardiac coil. T2 weighted single-shot fast spin echo (SSFSE) images were obtained to screen for unexpected pathology, to help characterize any lesions found post-gadolinium, and to estimate fat volume. Liver acquisition with volume

acceleration (LAVA) using 10 ml gadofosveset was performed with imaging parameters of: TR/TE/flip = 3.9/1.9/15, bandwidth = 125 kHz, slice thickness = 3 mm reconstructed at 1.5 mm intervals using twofold zero interpolation (ZIP 2), matrix = 512 X 512, and parallel acceleration factor = 2.

Post-processing: Conventional Reporting

3D surface rendering of the images was generated on a computer workstation (Advantage Windows, GE Medical Systems, Waukesha, WI). Two radiologists with experience levels of 1 and 4 years (SRB, NDT) in interpreting perforator studies performed the post-processing and interpretation. The rectus, gluteal, and posterior thigh muscle perforator artery sites of exit through the superficial muscle fascia were determined relative to the reference point. For deep inferior epigastric perforators (DIEP), the umbilicus served as the reference point. For gluteal artery perforators (GAP), a marker placed in the superior gluteal crease was the reference point, and for profunda artery perforators (PAP), the lowest point of the inferior gluteal crease was the reference point. Coordinates identifying the location of each perforating artery were displayed on a surface rendered image.

The radiologist reading the case measured perforator diameters at the site of penetration through the fascia using the Advantage Workstation as well as intramuscular course, length, and coordinates and manually entered the values in a report template. Flap volume estimates were calculated by designing the flap on the volume-rendered image. Our standard DIEP flap extended from 3 cm above the umbilicus down to 10 cm below the umbilicus. In the left–right direction, the flap was up to 40 cm wide, but not extending beyond the mid-axillary lines bilaterally at the level of the iliac crests. Posterior thigh flaps were 22–30 × 6 cm ovals on each side, starting just below the inferior gluteal crease. Inferior gluteal artery perforator (IGAP) flaps were again oval shaped and extended from the superior gluteal crease to the inferior gluteal crease. The horizontal width of these flaps was adjustable. The coordinates of perforators, diameters, intramuscular course description and length, fat volume, and additional details such as superficial inferior epigastric artery diameter are manually entered into a reporting template. An extended report with images of the individual arteries and 3D/MIP images is also provided to the surgeons as a courtesy.

Post-processing: Automated Reporting Software

The reporting software was implemented as a plugin for the OsiriX (v. 4.0, 32-bit) DICOM viewer running on a Macintosh computer (OS X 10.6.8). All programming was done in Objective-C, and the plugin is available for download at github.com/cjlang/pfara/releases. The software performed

the following eight major tasks for perforator quantification and reporting:

1. Perforator selection and coordinates estimation:

MRA blood pool phase data was loaded into the OsiriX DICOM viewer. The user marked the site of umbilical insertion into linea alba (reference point for DIEP flap reporting) with an electronic ROI point. Then, each candidate perforator was similarly marked at the site of perforation through the muscle sheath/fascia into the subcutaneous fat. The software automatically computed the coordinates of all the marked points and labeled them according to their superior/inferior and right/left coordinates in relation to the reference point.

2. Calculation of skin surface coordinates:

In abdominal cases, the lateral distance from the reference point for a given perforator was computed with a simple subtraction of coordinates. In gluteal cases, the radiologist drew a line along the skin surface to measure the distance from the reference point to the point on the skin posterior to the perforator ROI point (Fig. 2).

3. Intramuscular length estimation and course description:

Intramuscular length was calculated by a manual tracking method, where the operator marked points along the course of each perforator following its path through the muscle up to the point of joining a sufficiently large artery for performing micro-anastomosis (Fig. 3; here, all temporary ROI points are shown on a single image for illustration). The algorithm computes a summation of segment distances to produce an approximation of 3D intramuscular length using the standard Euclidean distance between two points:

$$\sum_{i=1}^p \sqrt{(x_i - x_{(i-1)})^2 + (y_i - y_{(i-1)})^2 + (z_i - z_{(i-1)})^2}$$

Here, p represents the number of temporary points with default labeling (e.g., “Point 1”) marked along the course of the perforator. The algorithm iterates over the images for each point, in order to identify the image containing the next point in the sequence (“Point i ” in the formula). This is necessary to support superior and inferior intramuscular course possibilities. On the first iteration of the summation (when $i = 1$), the coordinates of the original candidate perforator ROI point are used for the second term in each difference; this is the starting point for the length measurement. The summation ends with the final pair of points, and the resulting value represents the 3D Euclidean distance estimation. The software stores the vessel length measurement point coordinates from the axial view and later uses these coordinates to plot the course of the vessel on the volume-rendered image using an open

polygon and OsiriX spline rendering (Fig. 4). Utilizing the range of diameters for the current study, the open polygons illustrating the course of the vessels differ in width to provide a visual representation of relative perforator diameter. Lastly, the temporary points used to trace the course of the perforator in the axial view are automatically removed.

4. Flap volume estimation:

For estimating flap volume, the software assumes an elliptical flap geometry and uses SSFSE MR T2 weighted images to determine subcutaneous fat thickness. The fat volume within the oval range is segmented slice by slice based upon a pixel intensity thresholding method (Fig. 5). In an abdominal study, the region considered for fat volume estimation extended from 3 cm above to 10 cm below the umbilicus. The radiologist had the ability to adjust parameters for the fat segmentation; this includes altering the pixel intensity threshold for fat identification, as well as modifying the transverse and anteroposterior dimensions of the ROI rectangle (on the reference point image), defining the region within which to identify fat. Modification of the transverse dimension at the reference point image also scales all other rectangles in the transverse dimension by the same proportion; all rectangles have an equal anteroposterior dimension. Rectangles are scaled linearly in the transverse dimension as the algorithm moves superiorly and inferiorly from the reference point to the bounds of the fat estimation region; for example, with the default transverse dimension of 40 cm at the reference point, the rectangle will be 3 cm wide at the superior and inferior bounds of the fat estimation region. Fat regions are identified in a two-pass approach to each image within the fat region. Iterating over pixels within the image’s rectangle in both a left-to-right and right-to-left fashion, the algorithm looks for the initiation of a pixel sequence above the intensity threshold. This initiation triggers a brush ROI to begin painting the row of pixels within the image. Once the intensity falls back below the threshold, execution on that row terminates, the brush stops painting in that row of pixels, and iteration to the next row of pixels occurs. By approaching the rectangles from two directions, we are able to identify fat regions, while minimizing the risk of identifying high-intensity pixels that do not represent harvestable fat. Additionally, we experimented with a third approach in the anterior-to-posterior direction, but this did not provide meaningful benefit and, in some cases, mistakenly extended fat region identification beyond the fat wall. Once the plugin has completed painting the fat region within the flap, the radiologist has the option to touch up any missing regions or incorrectly identified regions of fat using the brush tool within OsiriX. As the entire process is highly subject to

Fig. 2 Screenshot of the plugin superimposed in axial T1 weighted post-contrast images demonstrating mapping of a gluteal perforator. The diameter and length of the vessel can be seen on the plugin interface as well as the rectangular bounds within the image, indicating the cropped image bounds



Fig. 3 Screenshot demonstrating intramuscular length calculation. The operator marks with ROI points the course of a single perforator in various slices along its path through the muscle up to the point of joining a sufficiently large artery for performing micro-anastomosis. Please note that all temporary ROI points in this example are shown on a single image for illustration

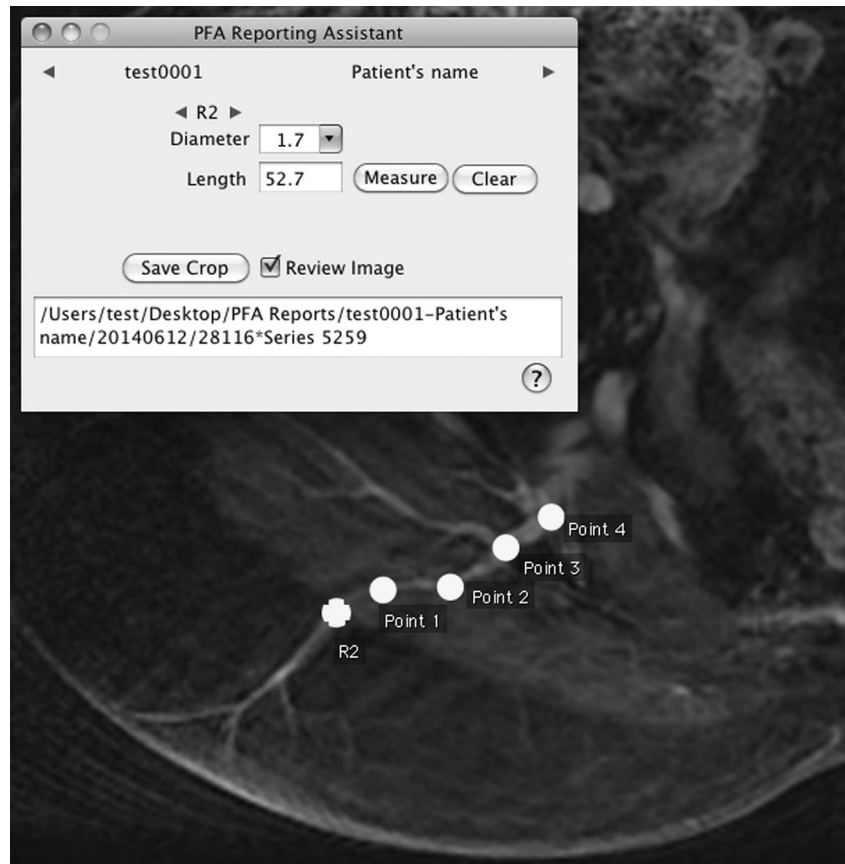


Fig. 4 Projecting perforating location and intramuscular course onto the skin surface on a volume rendered image

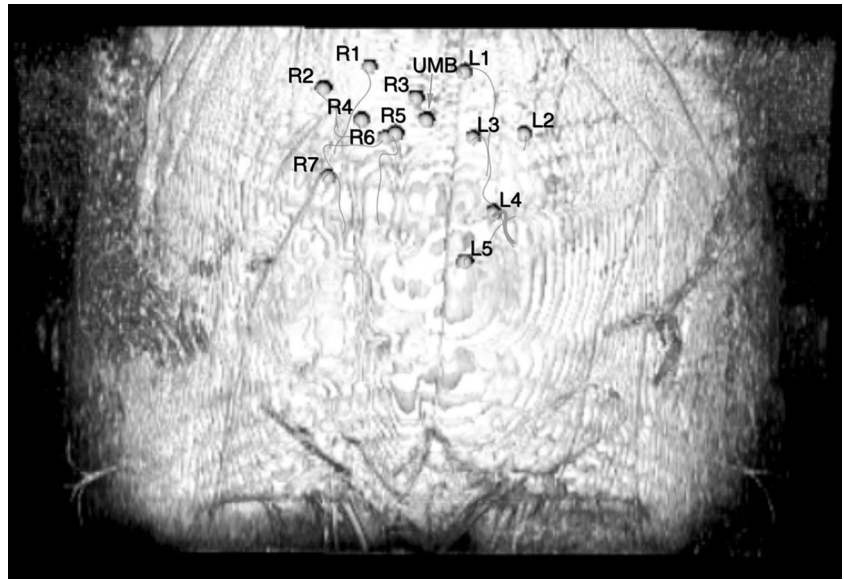


image quality, this feature gives the flexibility to manually correct the region if necessary.

Once all regions are identified via ROI within OsiriX, the algorithm computes the total fat volume using the following summations:

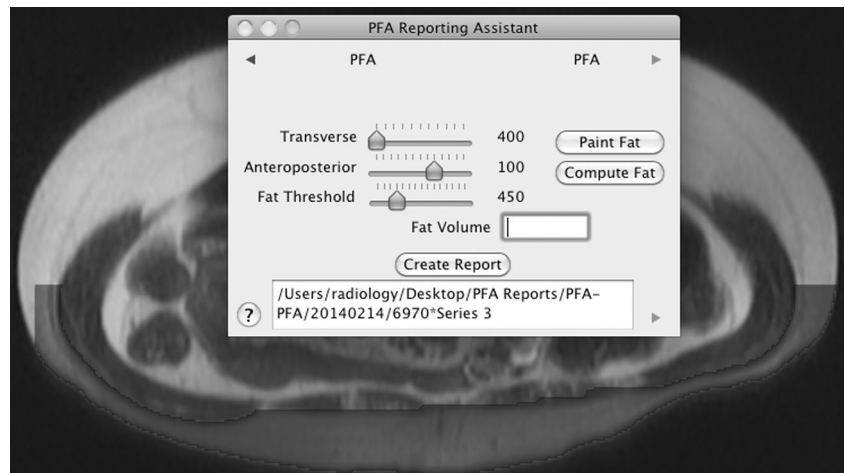
$$\text{Fat Volume (cc)} = \sum_{x=-s}^i \sum_{r=1}^b \left(a_{r,x} * \frac{t * f}{10} \right)$$

The inner summation iterates over brush ROIs (r) for a single image; there will be at least one brush ROI on each image within the fat segmentation region as long as that image contains at least one pixel identified as fat within the harvestable region; when $b > 1$, the radiologist has manually drawn on the image with an additional brush ROI. With each image, the fat volume is computed by directly taking the area of the brush ROI (a) in cm^2 and multiplying it by slice thickness

(t) in cm. The relationship between slice thickness and the defined flap region (3 cm superior and 10 cm inferior to umbilicus) determine the number of slices to use on either side of the reference image. Should this relationship be non-integer, the appropriate fraction of the most superior and/or most inferior image is determined and f is used to scale the fat volume computed at these boundary images by this fraction. For all other images within the fat segmentation region, $f = 1$.

The outer summation iterates over the images containing the fat segmentation region. Iteration occurs in a superior to inferior order, with $s =$ superior offset in number of images from the reference image, $i =$ inferior offset in number of images from the reference image, and when $x = 0$, the summation is on the reference point image. Automatically calculating flap volume estimates on CT images is still being developed.

Fig. 5 Fat segmentation range for anterior abdominal fat on axial view



5. Projecting perforating location/course onto the skin surface:

The skin surface boundary is defined using image gradient operator. To project perforator points to the skin in the axial plane, the plugin searches anterior and posterior from the ROI point toward the boundaries of the image. Via a pixel intensity threshold method, the skin is identified and new ROI points are created at these bounds. Creating a 3D volume-rendered image now displays these points on the skin region. By saving the 3D view in a standard size two-dimensional (2D) DICOM image, we can plot labels next to their corresponding points via a coordinate transform between the original axial view and the new 2D representation of the volume-rendered image. To do so, we utilize the original 2D x-coordinate, the index of the slice containing the ROI point, the total number of slices, and the boundary of the volume rendering within the DICOM image. Coordinates of the temporary points used to estimate intramuscular length are now transformed via the same method to plot a visualization of the course on the volume-rendered image using an open polygon and spline rendering within OsiriX (Fig. 4). These images and coordinates help the plastic surgeon locate the perforator arteries during pre-operative surface marking and intra-operatively.

6. Maximum intensity projection images of the main artery and branching pattern:

Coordinates identifying the location of the perforating arteries on the axial images are transformed and displayed on a volume-rendered 3D reconstructed image as described above and similarly on a coronal 3D MIP image (Fig. 6). The MIP images assist in evaluating the patency of the main artery (deep inferior epigastric artery for DIEP flap, profunda femoral artery for PAP flap, and gluteal artery for GAP flap) and branching pattern of deep inferior epigastric artery [3].

7. Insertion of cropped MIP images of individual perforators into the report:

The radiologist defines MIP thickness settings, adds notations for additional ROIs, and defines crop bounds with a rectangle ROI. The plugin sets axial perspective zoom to a standardized level, exports a JPEG of the full field of view, and crops the JPEG using image coordinates of the rectangle ROI.

8. Final Report Creation:

A final report is generated via Applescript commands that output both case-standardized text with patient-specific values and images that were generated throughout the reporting process. The textual reports without images were reviewed again with the attending signing off and copied and pasted into the hospital PACS reporting software (GE Centricity and Nuance Powerscribe 360, Burlington, MA). The reports with images were saved

as portable document format (PDF) files and uploaded to the patient's electronic medical record (EMR) and lifeIMAGE® (Newton, MA), a secure imaging platform which can be accessed by physicians lacking access to our electronic radiology records. A copy of the report with images was also mailed to the referring surgeons as a courtesy. The surgeons usually displayed the printed copies in the operating room (OR) or accessed the images on lifeIMAGE® with a computer.

Patient Testing

For 26 anonymized deep inferior epigastric artery perforator (DIEP) flap MRA studies that were reported conventionally using standard radiology reporting tools on a computer workstation (Advantage Windows 4.2, GE Waukesha, WI), the automated OsiriX plugin software reported them for comparison. For all cases, the reporting time was recorded. Following surgery, the OR times and information about complications were collected from OR notes and follow-up care notes. We compared the conventional reporting method to the newly developed computer-based reporting system using reporting time and accuracy of OsiriX as primary endpoints ($n = 26$). Conventional reports were analyzed for transcription errors. Subsequently, over 300 studies were reported with the new system only from June 2014 to November 2016.

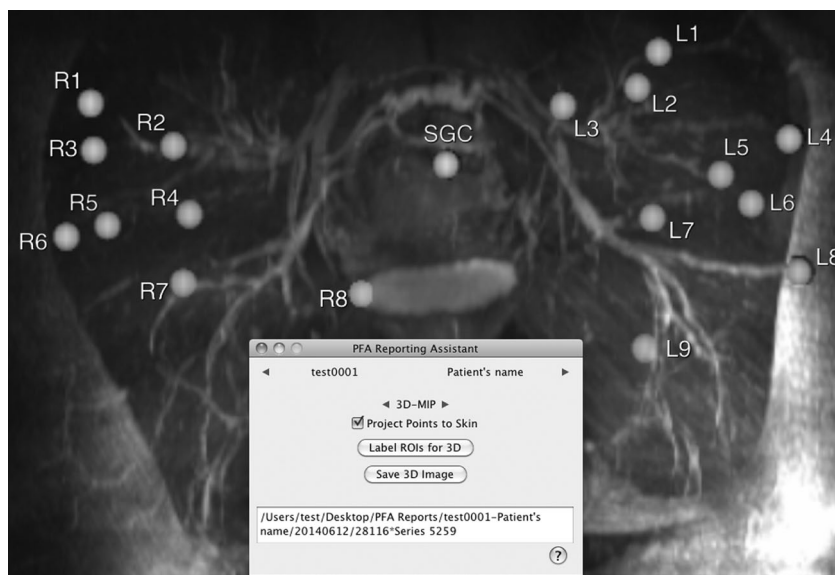
Statistical Testing

Statistical analysis of the difference in reporting time was performed by using a Mann–Whitney U test, as the manual reporting times were not normally distributed. The comparative analysis of perforator locations recorded as exact values was performed using paired t test. The magnitudes of correlation between the fat volumes were assessed with Pearson coefficient. All statistical analyses were performed with the use of GraphPad software (Prism version 6.00 for Mac OS X; GraphPad, La Jolla, CA). A P value of <0.01 was accepted as statistically significant.

Results

The mean reporting time using the conventional method (without plugin) was 76 ± 27 min (median 65 min) compared with 25 ± 6 min (median 25 min) using our latest OsiriX plugin ($p < 0.01$, U value 0, Z -score: 6.18) for the cases read by our radiologists. This version of the plugin reduced the mean time by approximately 47% compared with the mean processing time of a previous plugin (47 ± 8 min, median 45 min, U value 6 and Z -score 6.13 with $p < 0.01$, the result

Fig. 6 Maximum intensity projection images of the main artery and branching pattern



statistically significant) [7]. The intramuscular distance using the plugin was accurate to 0.5–1 cm in all cases. There were no false negatives or false positives. Of the 26 reports created manually, three (11.5%) had manual entry errors that were rectified during comparison with the OsiriX report.

The plugin was used for reporting DIEP MRA cases in this study. The plugin has been expanded for use in PAP, GAP, and CTA, but the small number of patients limits the available data and our ability to compute the plugin's utility for those cases.

The automated reporting software predicted flap volumes (456 cm^3 to 2012 cm^3 , mean = 1114 cm^3) that correlated well (Pearson correlation coefficient $r = 0.97$) with surgically harvested flaps (444 cm^3 to 2234 cm^3 , mean = 1088 cm^3). The initial flap design plan based on MRA was used for surgery in all (100%) of the cases. Partial flap necrosis was seen in two cases out of 102 pre-operative MRA studies performed between June and December 2014 (2%), which is a favorable rate compared to the historical flap necrosis incidence, 14% without pre-operative mapping [1].

The operative notes and feedback from plastic surgeons indicate that automated calculation and recording of perforator coordinates was accurate and more reliable than manually marking coordinates due to the elimination of data entry errors.

Discussion

Pre-operative imaging of perforators by CTA and MRA is a convenient and reliable tool for accurate pre-operative mapping of the vascular supply to flaps. It helps surgeons make informed choices, reduces operating room time, and lowers complication rates. MRA and/or CTA has become routine prior to this microsurgery. However, this new popularity of

perforator CTA and MRA has created workflow issues due to the tedious task of reporting perforator details with precise coordinates. Several software techniques including the use of OsiriX for 3D mapping of the perforator arteries have been reported [8–13]. However, to our knowledge, this is the first report of an automated plugin developed exclusively for perforator mapping which created a complete report, thereby making the pre-operative imaging more accessible to radiologists and solving several workflow-related issues. This automated OsiriX reporting system plugin accurately measured and reported perforator coordinates in a fraction of the time required previously. The faster and more accurate automated system has also led to reporting more perforators, thereby giving the plastic surgeons additional options for pre-operative selection of the best perforator.

Advantages of the automated system include low-cost, operational familiarity to Macintosh users, elimination of transcription errors, and a significant reduction in time spent by the radiologist. Finished reports are immediately available in electronic form. The images can also be simultaneously incorporated in the same Mac workstation eliminating the multiple steps required for manually incorporating images into the report on a PC or Mac. With increasing experience, preliminary reports generated by radiology assistants can be reviewed later by attending radiologists. The system also promotes a uniform reporting style. The plugin is user-friendly, and the surgeons can use it independent of a radiology report intra-operatively for any change in surgical planning. The OR time can be reduced by removing the need to contact an on-call radiologist.

A limitation of the plugin is that poor image quality may detract from the ability of the plugin to identify fat within the harvestable region. In addition, when points are projected to the skin for viewing on the 3D volume rendered image and

identifying labels are automatically placed near them, each label's placement is a standardized offset from its corresponding point's coordinates, which may result in overlap among labels and points. Another limitation exists when estimating intramuscular length; the accuracy of the measurement depends heavily on the temporary points marked by the radiologist. Finally, the fat segmentation cannot be used on CT images.

Conclusion

Perforator flap reconstruction is an important surgical breast reconstruction method after mastectomy. A radiology report needs to provide precise perforator coordinates/dimensions, perforator course, and fat volume to help the plastic surgeon plan and perform the surgery. Manual measurement and reporting of these perforator geometric parameters is tedious and takes hours. Automatic perforator reporting software has been implemented as an OsiriX DICOM viewer plugin to assist in measuring and reporting perforator geometry, including the umbilicus or similar reference point and perforating artery/vein course definitions beginning at the muscle–fat interface. This perforator software can help to reduce radiology reporting time threefold.

References

1. Minqiang X, Lanhua M, Jie L, Dali M, Jinguo L. The value of multidetector-row CT angiography for pre-operative planning of breast reconstruction with deep inferior epigastric arterial perforator flaps. *Br J Radiol*. 2010;83(985):40–3.
2. Rozen WM, Ashton MW. Modifying techniques in deep inferior epigastric artery perforator flap harvest with the use of pre-operative imaging. *ANZ J Surg*. 2009;79 (9):598–603
3. Zou Z, Kate Lee H, Levine JL, Greenspun DT, Allen RJ et al. Gadofosveset trisodium-enhanced abdominal perforator MRA. *J Magn Reson Imaging*. 2012;35 (3):711–6.
4. Masia J, Clavero JA, Larrañaga JR, Alomar X, Pons G, Serret P. Multidetector-row computed tomography in the planning of abdominal perforator flaps. *J Plast Reconstr Aesthet Surg* 2006; 59: 594–9.
5. Agrawal MD, Thimmappa ND, Vasile JV, Levine JL, Allen RJ et al. Autologous breast reconstruction: pre-operative magnetic resonance angiography for perforator flap vessel mapping. *J Reconstr Microsurg*. 2015; 31(1):1–11
6. Eylert G, Deuting M, Stemberger A, Huber W, Gösseringer N. Evaluation of the perforator CT-angiography with a cancer risk assessment in DIEP flap breast reconstruction. *J Plast Reconstr Aesthet Surg*. 2015;68(4):e80–2.
7. Thimmappa, N, Pei, M, Wang, Y, Chen, C, Ahn, C et al., Semi-automated perforator flap reporting. Radiological Society of North America 2012 Scientific Assembly and Annual Meeting, Chicago IL. <http://archive.rsna.org/2012/12023099.html> Accessed November 10, 2016.
8. Chae MP, Hunter-Smith DJ, Rozen WM. Comparative study of software techniques for 3D mapping of perforators in deep inferior epigastric artery perforator flap planning. *Gland Surg*. 2016;5(2): 99–106
9. Eder M, Raith S, Jalali J, Müller D, Harder Y, et al. Three-dimensional prediction of free-flap volume in autologous breast reconstruction by CT angiography imaging. *Int J Comput Assist Radiol Surg*. 2014;9(4):541–9
10. Hummelink S, Hameeteman M, Hoogeveen Y, Slump CH, Ulrich DJ, Schultze Kool LJ. Preliminary results using a newly developed projection method to visualize vascular anatomy prior to DIEP flap breast reconstruction. *J Plast Reconstr Aesthet Surg*. 2015;68(3): 390–4.
11. Zöllner FG, Daab M, Sourbron SP, Schad LR, Schoenberg SO, Weisser G. An open source software for analysis of dynamic contrast enhanced magnetic resonance images: UMMPerfusion revisited. *BMC Med Imaging*. 2016;16:7.
12. Blackledge MD, Collins DJ, Koh DM, Leach MO. Rapid development of image analysis research tools: bridging the gap between researcher and clinician with pyOsiriX. *Comput Biol Med*. 2016; 69: 203–12.
13. Lo Presti G, Carbone M, Ciriaci D, Aramini D, Ferrari M, Ferrari V. Assessment of DICOM viewers capable of loading patient-specific 3D models obtained by different segmentation platforms in the operating room. *J Digit Imaging*. 2015; 28(5):518–27.